Hyperspectral imaging system for in-vivo quantification of skin pigments

Pierre Seroul, Mathieu Hébert, Matthieu Jomier

Proceedings of the 28th IFSCC Congress, Paris, France, 123-132 (2014).

Hyper-spectral imaging system for in-vivo quantification of skin pigments

Pierre Seroul[a], Mathieu Hébert[b], Matthieu Jomier[a],

[a]Newtone Technologies, 17, cours de la Liberté, F-69003 Lyon, France.

[b]Université de Lyon, Université Jean Monnet de Saint-Etienne, CNRS UMR5516 Laboratoire Hubert Curien, 18 rue Benoît Lauras, F-42000 Saint-Etienne, France.

Abstract

We present a new multi-spectral imaging system, SpectraCam®, allowing the capture of in-vivo images of the skin over the whole visible spectrum under UV or white light. The use of cross-polarization enables removing light reflections of the stratum corneum, which may be an important error factor in chromophores quantification. An implementation of the Kubelka-Munk model combined with Saunderson correction allows measuring six parameters of Caucasian skin: epidermis thickness, melanin volume fraction, blood volume fraction, oxygen saturation and bilirubin volume fraction. Maps of these parameters can be displayed and different structures may be observed such as blood vessels, pores, hematoma or pigmented spots. An error map is also provided to highlight structure that do not fit will the developed skin reflectance model. All the results obtained have been correlated to previous results in the literature.

Introduction

Skin chromophores and their influence on skin color perception are of high concern in dermatology and cosmetics in order to evaluate pigmentation issues [1,2,3]. Non-invasive imaging systems of the skin are used in a wide range of clinical applications in the last decades, in particular in order to get information on pigmentation disorders: melanin index, port wine vein, vitiligo, erythema [4,5]… Since pigmentation determines the spectral reflectance of the skin, the best way to observe it is to make images in different spectral bands, either in three wide spectral bands as in classical RGB imaging, or in more than 10 short spectral bands as in multispectral imaging [6]. There already exists several multispectral imaging instruments for skin observation on the marketplace (e.g. SIAscope from Cosderma laboratories, or MelaFind from Mela Sciences, …) generally dedicated to specific measurements. Stamatas et al. [7] showed that the most accurate approach to measure concentrations of chromophores and photophores in the skin is to take into account their spectral absorbance. As far as we know, no company has already proposed such a hyper-spectral system including spectral absorbance of molecules in the domain of dermatology. In this paper, we present a new hyper-spectral imaging device, SpectraCam®, developed for chromophores and photophores measurement. It allows the acquisition of 93 images in different wavebands of the visible spectrum of light (400-700nm), where 62 images are used to the measurement of chromophores and 31 for the measurement of photophores, and enables extracting skin parameters such as blood,

melanin and bilirubin volume fractions, epidermis thickness, oxygen saturation. Using cross-polarized filters the light reflection by stratum corneum can be removed, in order to minimize distortion of the signal emitted by the chromophores.

The concentration and localization of chromophores in the skin cannot be measured directly by optical device. In order to deduce them from light signal captured by the imaging system, a model of light propagation in human tissues is needed. Two main approaches are usually followed in the literature, either based on Monte-Carlo simulation or on the Kubelka-Munk 2-flux model. The Monte-Carlo method consists in a stochastic stimulation of light paths in the skin with multiple interactions with particles [1]. The Kubelka-Munk model is a physical model of light propagation that can be seen as a special solution of the radiative transfer equation, standing in case of strong scattering [8]. This model has been used in a wide range applications, included skin analysis [9, 3] although the Saunderson correction that takes into account the optical effect of the air-skin interface [10] has never been introduced in these specific models.

Our method follows the second approach based on the Kubelka-Munk model with Saunderson correction, applied to a simplified model of skin tissues. We can retrieve several skin parameters with a satisfying level of reproducibility and generate maps of their distribution on the skin. We implemented a brute-force optimization in order to retrieve five parameters per pixel related to the optical properties of skin: epidermis depth, melanin volume fraction, blood volume fraction, oxygen saturation and bilirubin volume fraction. The estimation error between simulated and real spectrum is computed using spectral angle similarity (SAS) [11]. In order to verify the performance of the method, acquisitions were made on ten Caucasian skins to correlate results reported by previous works [12, 13].

In this paper, we first propose to recap the main lines of the Kubelka-Munk model, then to show how five characteristic parameters of skin can be measured using this model, and finally show the performance of the method through experimental results.

The Kubelka-Munk model

The Kubelka-Munk model describes the propagation of diffuse natural light within a layer of homogenous scattering and absorbing medium. It especially describes the attenuations due to absorption and to back-scattering of two fluxes propagating in opposite direction by infinitesimal sublayer.

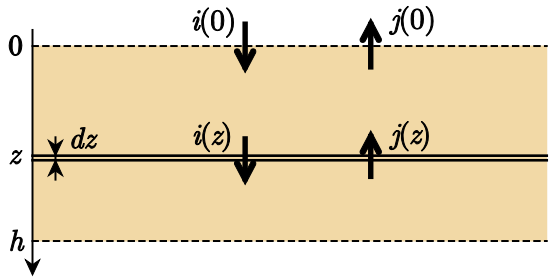

Figure 1. Upward and downward diffuse fluxes crossing a sublayer of thickness dz.

Let us consider a layer with thickness h, absorption coefficient K and scattering coefficient S. A diffuse flux denoted as i propagates downwards, and a diffuse flux denotes as j propagates upwards (Figure 1). At depth z in the layer, a sublayer with infinitesimal thickness dz receives the fluxes $i(z)$ on its top face, and $j(z+dz)$ on its lower face. Though the sublayer, flux $i(z)$ looses the flux $Ki(z)dz$ due to absorption (this lost flux is proportional to the incoming flux, the thickness of the sublayer, the proportionality factor being the absorption coefficient) and the flux $Si(z)dz$ that is backscattered and contributes to the upward flux (also proportional to the incoming upward flux and the thickness of the sublayer, the proportionality factor being the scattering coefficient); it also gains the upward flux $Sj(z+dz)dz$ that is backscattered by the sublayer. Likewise, the upward flux $j(z+dz)$ losses the flux $Kj(z+dz)dz$ due to absorption and the flux $Sj(z+dz)dz$ due to backs-cattering, and gains the backscattered downward flux $Si(z)dz$. One can thus write the two equations:

$$\begin{cases} i(z+dz) = i(z) - Ki(z)dz - Si(z)dz + Sj(z+dz)dz \\ j(z) = j(z+dz) - Kj(z+dz)dz - Sj(z+dz)dz + Si(z)dz \end{cases} \quad (1)$$

which can be transformed in the following ones, as dz tends to zero:

$$\begin{cases} \dfrac{di}{dz} = -(K+S)i(z) + Sj(z) \\ \dfrac{dj}{dz} = -Si(z) + (K+S)j(z) \end{cases} \quad (2)$$

Equations (2) correspond to the Kubelka-Munk differential equation system.

When a function has a Laplace transform, this latter is unique. The converse is also true. Since $p/\left(p^2 - b^2S^2\right)$ and $bS/\left(p^2 - b^2S^2\right)$ are the respective Laplace transforms of $\cosh(bSz)$ and $\sinh(bSz)$ [17], one concludes that $I(p)$ and $J(p)$ are the respective Laplace transforms of

$$i(z) = i(0)\cosh(bSz) + \frac{1}{b}\left[j(0) - ai(0)\right]\sinh(bSz) \quad (3)$$

and

$$j(x) = j(0)\cosh(bSx) + \frac{1}{b}\left(aj(0) - i(0)\right)\sinh(bSx) \quad (4)$$

Expressions (4) and (3) are the general solutions of the Kubelka-Munk differential equation system. Special solutions can be obtained by considering boundary conditions corresponding to the fluxes received on the faces at $z = 0$ and $z = h$. In the basic case, the top face receives a flux I and the back side is not illuminated. Therefore, one has

$$i(0) = I_0 \quad (5)$$

and

$$j(h) = 0 \quad (6)$$

By inserting these boundary conditions into Eqs. (3) and (4), one obtains the reflectance R of the layer, defined as the ratio of outgoing flux at the top side to incident flux, therefore the ratio $j(0)/I$:

$$R = \frac{\sinh(bSh)}{b\cosh(bSh) + a\sinh(bSh)} \tag{7}$$

with

$$a = (K + S)/S \quad \text{and} \quad b = \sqrt{a^2 - 1} \tag{8}$$

The transmittance of the layer, defined as the ratio of outgoing flux on the back side to the incident flux, therefore the ratio $i(h)/I$, is given by

$$T = \frac{b}{b\cosh(bSh) + a\sinh(bSh)} \tag{9}$$

As the thickness of the layer tends to infinity, the reflectance tends to the limit

$$R_\infty = a - b = \frac{K + S - \sqrt{K(K + 2S)}}{S} \tag{10}$$

and the transmittance obviously tends to 0.

When the layer is on top of a background with reflectance ρ_g, one has the boundary condition at $z = h$:

$$j(h) = \rho_g i(h) \tag{11}$$

Eqs. (3) and (4) with the boundary conditions (6) and (11) yield the following reflectance expression:

$$R_g = \frac{(1 - \rho_g a)\sinh(bSh) + \rho_g b\cosh(bSh)}{(a - \rho_g)\sinh(bSh) + b\cosh(bSh)} \tag{12}$$

Note that since absorption and scattering coefficients generally depend on wavelength, all reflectance and transmittance expression also depend on wavelength.

Saunderson correction

Most of the time, the refractive index of the layer is different from the one of the surrounding medium, e.g., air. In this case, the boundary condition at the top face $z = 0$ must take into account the Fresnel reflections and transmission of light at the air-medium interface (independent of the wavelength except in case of strong dispersion, which is not the case in the present domain of application). A fraction r_s of the incident flux I may be reflected towards the detection device while a fraction T_{in} penetrates the layer. Regarding the upward flux at $z = 0$, a fraction T_{out} of it goes out in air and a fraction r_i is back reflected into the layer. The outgoing flux in air is denoted as J. One thus has

$$i(0) = T_{in} I + r_i j(0) \tag{13}$$

and

$$J = r_s I + T_{out} j(0) \tag{14}$$

The reflectance expression for the layer with background and interface with air, given by inserting the boundary conditions (11), (13) and (14) into Eqs. (3) and (4), may be written:

$$R_S = r_s + \frac{T_{in} T_{out} R_g}{1 - r_i R_g} \tag{15}$$

where R_g is given by Eq. (12).

This expression generalizes the Saunderson correction for the Kubelka-Munk model for any measuring geometry (in his original paper, Saunderson considered illumination at 45° from the normal of the layer, and observation in the normal of the layer [10]). The terms r_s, T_{in} and T_{out} depend on the measuring geometry [18], but it has been shown that these terms are almost not modified by eventual roughness of the surface [20]. For the 8°:0°geometry, one has

$$r_s = R_{fresnel}(\theta_{ill})$$
$$T_{in} = T_{fresnel}(\theta_{ill}) = 1 - R_{fresnel}(\theta_{ill})$$
$$T_{out} = T_{fresnel}(\theta_{obs}) / n^2$$

where θ_{ill} and θ_{obs} respectively denote the angles of illumination and observation, n is the refractive index of the layer and the factor $1/n^2$ introduces the fact that the captured radiance has been spread into a larger cone when crossing the interface due to refraction [18]. Note that $r_s = 0$ when $\theta_{ill} \neq \theta_{obs}$; it is also zero when the specular reflection is removed by polarization filtering.

Simplified skin model

Human skin may be approximated as a two-layer system: epidermis and dermis. The epidermis is a diffusing layer with refractive index n = 1.4, thickness h, absorption coefficient K_e and scattering coefficient S_e. Below the epidermis, the dermis is a diffusing layer with absorption coefficient K_d and scattering coefficient S_d. Its thickness is assumed infinite and its refractive index identical to the one of the epidermis. In this skin model, we have a diffusing layer on top of a background: its reflectance is therefore expressed by Eq. (15). It is surprising to see that, as far as we could see in the literature dedicated to medical applications of the Kubelka-Munk model for skin, the Saunderson correction is almost always ignored, which is contradiction with the physical laws and introduces significant error in the skin reflectance model. This is why we prefer introducing the Saunderson correction in our model. Note that the flux reflections and refractions at the epidermis-air interface are taken into account in the model by Magnain & al. based on the radiative transfer equation solved using the auxiliary function method [21].

For the spectral scattering coefficients of the epidermis and dermis, and the spectral absorption coefficients of the skin pigments used in our model, we referred to Ref. [12]. The absorption coefficients of the two layers depend on the pigments contained in them and their respective volume fraction: the absorption coefficient of a mixture of components is generally the sum of the absorption coefficients of the components, weighted by their respective concentration [22].

The epidermis contains a baseline with absorption coefficient $K_b(\lambda)$, and melanin with absorption coefficient $K_m(\lambda)$ and volume fraction c_m. The absorption coefficient of the epidermis is therefore

$$K_e(\lambda) = (1 - c_m) K_b(\lambda) + c_m K_m(\lambda) \tag{16}$$

With this absorption coefficient $K_e(\lambda)$ and the scattering coefficient $S_e(\lambda)$, the reflectance R_e and transmittance T_e of the epidermis can be computed as a function of its thickness h using Eqs. (7) and (9).

The dermis contains the same baseline as the epidermis [absorption coefficient $K_b(\lambda)$], deoxy-hemoglobin Hb (absorption coefficient $K_{Hb}(\lambda)$ and volume fraction c_{Hb}), oxy-hemoglobin Hb02 ($K_{Hb02}(\lambda)$, c_{Hb02}) and bilirubin ($K_{bi}(\lambda)$, c_{bi}):

$$K_d(\lambda) = c_b K_b(\lambda) + c_{Hb} K_{Hb}(\lambda) + c_{Hb02} K_{Hb02}(\lambda) + c_{bi} K_{bi}(\lambda) \tag{17}$$

with $c_b = 1 - (c_{Hb} + c_{Hb02} + c_{bi})$. With this absorption coefficient K_d and the scattering coefficient S_d, the reflectance R_d of the dermis can be computed using Eq. (10).

SpectraCam®: a new hyperspectral device

SpectraCam® is a modular device for hyperspectral imaging. In its standard mode, it can capture up to 31 images in different thin wavebands of the visible spectrum (400–700 nm), every 10 nm. For specific clinical application, the device can also capture one image every 1 nm through a spectral band of 10 nm.

In order to avoid perturbation of the images by the gloss due to the reflection of light by the surface of the skin, the system contains a two polarization filters, one for polarizing the incident light, the other one to filter the reflected light. This system uses the fact that when the incident light is polarized, the light reflected by the air-medium interface (i.e., the gloss) as the same polarization than the incident light, whereas the light scattering into the diffusing medium is unpolarized. Thus, when the second polarizing filter is parallel to the first one (Parallel-Polarization mode, PP), it transmits both the gloss and the diffused light. When it is perpendicular to the first filter (Cross-Polarization mode, CP), it transmits only the diffused light and gloss is removed.

For chromophores measurement, the cross-polarization mode is selected in order to remove gloss that usually appears at the surface of the stratum corneum. For skin surface analysis, the parallel-polarized lighting system is selected: gloss parameters are obtained by comparing cross-polarized and parallel-polarized images (Figure 2).

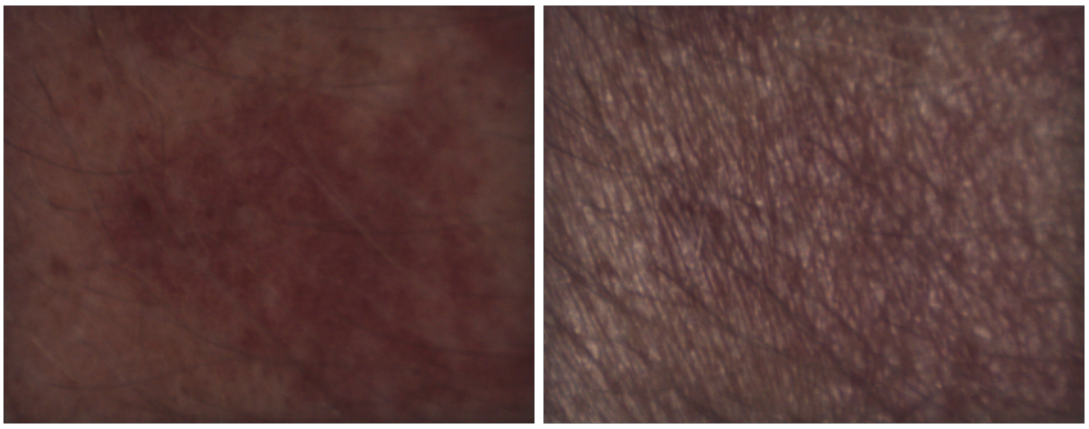

Figure 2 - Comparison between images of a same skin area captured in cross-polarization and parallel-polarization modes (the multispectral images converted into RGB color images). CP images allows good quantification of pigments, PP allows visualization of the surface topology.

The SpectraCam® device also contains a UV-A lamp emitting at 365 nm which can be used for photophores analysis. 31 images are captured corresponding to the same wavelength as for the chromophores analysis, in cross-polarization mode. In the case where the UV lamp is on, the measured spectrum does not rigorously correspond to a spectral reflectance but rather to the sum of spectral reflectance and a spectral emittance (due to the photophores). However, this distinction has no conceptual or practical consequence in the following of our study.

The repeatability of the spectral measurement system is similar to spectrophotometers used in color reproduction: the standard deviation over 10 measurements on a same white ceramic, expressed in CIELAB 1976 ΔE^*_{ab}, is 0.09 unit with our system, therefore comparable to the Konica Minolta CM-700d instrument (0.04 unit on the same sample) and the X-Rite SP62 instrument (0.05 unit).

Computation of the skin parameters from measured spectra

The spectral reflectance of the skin is given by Eq. (15), with $R_g(\lambda)$ given by Eq. (12). In the expression of $R_g(\lambda)$, the background reflectance $\rho_g(\lambda)$ is replaced with the dermis reflectance $R_d(\lambda)$ expressed by Eq. (10) as a function of $S_d(\lambda)$ and $K_d(\lambda)$ [Eq. (17)]; the reflectance R and transmittance T of the epidermis are respectively expressed by Eqs. (7) and (9) as functions of $S_e(\lambda)$ and $K_e(\lambda)$ [Eq. (16)]. For each pixel of the multispectral image, one fits the pigment concentrations and the epidermis thickness as values for which the Spectral Angle Similarity (SAS) [25] between the spectrum $R_p(\lambda)$ predicted by our reflectance model and the measured spectrum $R_m(\lambda)$ is minimal:

$$\{c_m, c_{Hb}, c_{Hb02}, c_{bi}, h\} = \underset{c_m, c_{Hb}, c_{Hb02}, c_{bi}, h}{\arg\min} \arccos\left(\frac{\sum R_p(\lambda) R_m(\lambda)}{\left[\sum R_p^2(\lambda)\right]\left[\sum R_m^2(\lambda)\right]}\right)$$

The fact that the different pigments have different absorption bands insures a unique solution for this optimization process. In order to verify the stability of the obtained

values of parameters, we introduced small variations in the multispectral image and observed that the variations of the parameter values were low. Moreover, we could verify that there exists a bijective relationship between the parameter values and the reflectance spectra, which means that the model can be reversed. This enables attributing a unique set of parameters to every reflectance spectrum of skin. However, the spectrum predicted with the set of parameters, even optimal, may differ from the measured one. In order to assess this deviation, the SAS metric was computed for each pixel of the multispectral image. The deviations highlighted with this metric may come from the presence of other pigments, unexpected optical phenomena, or local variations of the optical propertied of the skin that are not taken into account in our model.

Experimental testing

Clinical experiments were performed onto 10 Caucasian subjects with phototypes I to III on the Fitzpatrick scale [23,24], 5 males and 5 females between 20 and 50 years old. Seven areas of interest were observed on each subject, located on the right and left inner forearms, on the right and left cheeks and on the forehead. This makes a set of 70 multispectral images. The size of each area is 3.5 cm x 3.5 cm (1350 x 1350 pixels). Average skin parameters and their standard deviation, obtained from the 70 multispectral images, are given in Table 1. An originality of our study is the measurement of the bilirubin volume fraction by multispectral imaging. The SAS value computed over all pixels of the 70 multispectral images was 0.044, which is of the same order as the value 0.017 given in Ref. [3].

Table 1. Skin parameters measured from 7 areas on 10 Caucasian subjects

Skin Parameter	Measured value*	Data from the literature
Epidermis thickness	41 ± 8 μm	34 ± 4 μm [15]
Melanin volume fraction	15 ± 5.7%	1.3 – 43% [12]
Blood volume fraction	5.5 ± 3.7%	2 − 5% [12]
Oxygen saturation	50 ± 15%	25−90% [16]
Bilirubin volume fraction	0.35 ± 0.15%	0.3−1.2 mg/dL [14]**

*Average over the 10 Caucasian subjects and standard deviation

**This concentration of biliburin is measured in serum whereas our measurement is an effective volume fraction in the skin.

Multispectral imaging is convenient for 2D display of the variations of each parameter in the observed area. Figure 3 shows an example of observed skin area, with a color image and 6 grey-level images representing maps for the five skin parameters and SAS value. For example, the position of the blood vessels, just noticeable in the color image, is emphasized in the blood concentration map (Figure 3.a). Freckles and color variations can be observed in the melanin concentration map (Figure 3.c). The SAS map highlights regions in the image where the predicted spectrum with the set of fitted parameters deviates more from the measured spectrum; it may indicate the presence of unexpected substances, optical phenomena or skin properties.

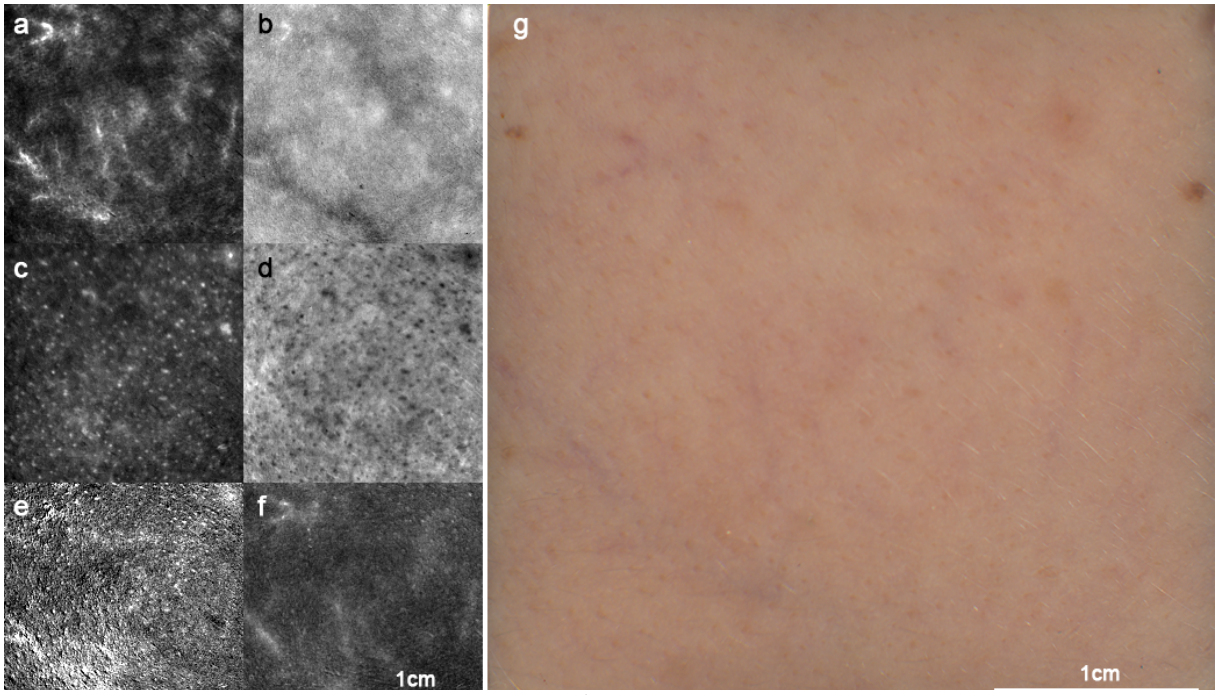

Figure 3. Observation of a piece of female check issued from multispectral measurement in cross-polarization mode, including maps of (a) blood volume fraction, (b) oxygen saturation, (c) melanin volume fraction, (d) epidermis thickness, (e) bilirubin volume fraction, (e) SAS and (g) color.

Conclusions

The SpectraCam® device presented here allows good characterization of the human skin. A far as we known, it is the first available device capturing in-vivo images of the skin over the whole visible spectrum under fluorescent or white light. The use of cross-polarization enables removing light reflections of the stratum corneum, which may be an important error factor in chromophores quantification. The model that we use to extract the skin parameters from the multispectral images is the Kubelka-Munk model with Saunderson correction. While the Saunderson correction seems to be ignored in most existing works, its use guarantees better accuracy. The model allows retrieving six parameters of Caucasian skin: epidermis depth, melanin volume fraction, blood volume fraction, oxygen saturation and bilirubin volume fraction. The measurement of this latter parameter is also an originality of our work compared to the existing works. Maps of each of these parameters can be displayed to observe different structures such as blood vessels, pores, hematoma or pigmented spots. A spectral deviation map is also displayed to highlight structures that do not fit well with the developed skin model. From the tests carried out in this study, we observed good agreement between the parameter values measured with our system and those available in the literature. Thus, we think that the SpectraCam®, combined with the algorithm presented in this paper, can be an efficient tool for early diagnosis of skin lesions. In the future, we would like to correlate the measured parameters values with ex-vivo analysis of the same region of interest after excision.

References

1. Preece, S.J., Claridge, E. (2004). "Spectral filter optimization for the recovery of parameters which describe human skin." *IEEE Trans. Pattern Anal. Mach. Intell* **26**, 913–922.
2. Cotton, S. (1997). "A noninvasive skin imaging system", in *Information Processing in Medical Imaging*, Duncan J. and Gindi G. Eds., *Lecture Notes in Computer Science* **1230**, Springer, Berlin, pp. 501-506.
3. Jolivot R. (2011). *Development of an imaging system dedicated to the acquisition, analysis and multispectral characterisation of skin lesions*, PhD dissertation at the Université de Bourgogne.
4. Nilsson, G. (2014). "Tissue Viability Imaging for Assessment of Skin Erythema and Blanching" *Non Invasive Diagnostic Techniques in Clinical Dermatology*, 187-199.
5. Jung, B., Choi, B., Durkin, A.J., Kelly, K.M., Nelson, J.S. (2004) "Characterization of Port Wine Stain Skin Erythema and Melanin Content Using Cross-Polarized Diffuse Reflectance Imaging," *Lasers in Surgery and Medicine* **34**, 174-181.
6. Elbaum, M. (2002). "Computer-Aided Melanoma Diagnosis" *Dermatologic Clinics* **20**, 735-47.
7. Stamatas, G.N., Zmudzka, B. Z., Kollias, N., Beer, J. Z. (2004). "Non-invasive measurements of skin pigmentation in situ". *Pigment Cell Res.* **17**, 618–626.
8. Kubelka, P. (1948) "New contributions to the optics of intensely light-scattering material, part I," *J. Opt. Soc. Am.* **38**, 448–457.
9. Igarashi, T., Nishino, K., Nayar, S. K. (2007). "The appearance of human skin: A survey," *Found. Trends. Comput. Graph. Vis.*, **3** (1), 1–95.
10. Saunderson, JL. (1942) "Calculation of the color pigmented plastics," *J. Opt. Soc. Am.* **32**, 727–736.
11. Yuhas, R., Goetz, A., Boardman, J. (1992). "Discrimination among semi-arid landscape endmembers using the spectral angle mapper (sam) algorithm" *Summaries of the Third Annual JPL Airborne Geoscience Workshop*, I (JPL Publication 92-14), 147–149 .
12. Jacques (1998), *Skin optics*. Oregon Medical Laser Center News.
13. Huzaira, M., Rius, F., Rajadhyaksha, M., Anderson, R., Gonzalez, A. (2001). "Topographic Variations in Normal Skin, as Viewed by In Vivo Reflectance Confocal Microscopy," *The journal of Investigative Dermatology* **116** (6), 846–852.
14. Puppalwar1, P.V., Goswami, K., Dhok, A. (2012). "Evolution of Methods of Bilirubin Estimation," *Journal of Dental and Medical Sciences* **1** (3), 17-28
15. Corcuff, P., Bertrand, C., Lévêque, JL. (1993) "Morphometry of human epidermis in vivo by real-time confocal microscopy." *Arch Dermatol Res.* **285**, 475–481.
16. Meglinsky, I., Matcher, S. (2001). "Modelling the sampling volume for skin blood oxygenation measurements," *Medical and Biological Engineering and Computing* **39**, 44–50.
17. Abramovitz, M., Stegun, IA. (1964) *Handbook of mathematical functions with formulas, graphs, and mathematical tables*, Dover, New-York, pp. 1022–1023.
18. Simonot, L., Hébert, M., Hersch, R.D. (2006). "Extension of the Williams-Clapper model to stacked nondiffusing colored layers with different refractive indices," *J. Opt. Soc. Am. A* **23**, 1432–1441.
19. Judd, D.B. (1942). "Fresnel Reflection of Diffusely Incident Light," *J. Res. Natl. Bur. Stand.* **29**, 329–332.
20. Hébert, M., Hersch, R.D. (2005). "Extending the Clapper–Yule model to rough printing supports," *J. Opt. Soc. Am. A* **22**, 1952–1967.
21. Magnain C., Elias M., Frigerio J.M. (2007). "Skin color modeling using the radiative transfer function solved by the auxiliary function method," *J. Opt. Soc. Am. A* **24**, 2196–2205.
22. Kortüm, G. (1969) *Reflectance Spectroscopy, Principles, Methods, Applications*, Springer-Verlag, Berlin.
23. Fitzpatrick, T. B. (1975) "Soleil et peau", *Journal de Médecine Esthétique* **2,** 33–34 (in French).
24. Fitzpatrick, T. B. (1986). "Ultraviolet-induced pigmentary changes: Benefits and hazards", *Therapeutic Photomedicine* **15**, 25-38.
25. Kruse, F.A., Boardman, J.W., Lefkoff, A.B., Heidebrecht, K.B., Shapiro, A.T., Barloon, P.J., Goetz, A.F.H., (1993) "The Spectral Image Processing System (SIPS)—interactive visualization and analysis of imaging spectrometer," *Data. Remote Sens. Environ.* **44**, 145-163.